Detection of magnetic barriers in a chaotic domain: first application of Finite Time Lyapunov Exponent method to a magnetic confinement configuration

G. Rubino[1], D. Borgogno[2], M. Veranda[3], D. Bonfiglio[3], S. Cappello[3], D. Grasso[1]

[1] Istituto dei Sistemi Complessi-CNR, Politecnico di Torino, Corso Duca degli Abruzzi 24, 10129 Torino, Italy

[2] Université de Nice-Sophia Antipolis, CNRS, Observatoire de la Cote d'Azur, BP 4229, 04304 Nice Cedex 04, France

[3] Consorzio RFX (CNR, ENEA, INFN, Università di Padova, Acciaierie Venete SpA) Corso Stati Uniti 4, 35127 Padova (Italy)

Abstract

Magnetic field lines embedded in a plasma confinement system are often characterized by a chaotic motion. This weakens the confinement properties of any magnetic configuration. However, even in case of chaotic domains, magnetic barriers can emerge and limit the field line motion itself. In the context of the numerical simulation of a Reversed-Field Pinch configuration a new magnetic topology analysis, borrowed from previous fluid dynamic studies, is here discussed. This methodology relies on the behavior of the Finite Time Lyapunov Exponent (FTLE) associated with the magnetic field. By referring to a previous work [D. Borgogno et al., *Phys. Plasmas* **18** 102307, 2011], where the magnetic field is given in terms of analytical functions, in case of magnetic barriers the FTLE field shows the presence of ridges, special gradient lines normal to the direction of minimum curvature. These ridges can be recognized as Lagrangian Coherent Structures (LCSs) for the system, actually opposing the penetration of magnetic field lines across them. In this paper a more general numerical scheme for the detection of the LCSs has been adopted, which allows to analyze realistic cases where the magnetic fields are numerically known on a discrete mesh. After a validation test performed on the analytical case, a first application to a numerical magnetohydrodynamics simulation of the RFP, characterized by a broad chaotic region, has been performed. A strong magnetic barrier has been observed that effectively limits the field lines motion inside the chaotic sea.

I. INTRODUCTION

The understanding of the mechanisms leading to transport barriers formation is a common interest in ordinary fluids and hot plasmas [1–6]. In the case of hot laboratory - magnetically confined - plasmas for thermonuclear fusion research the barrier formation leads to improved confinement properties and thus constitutes a subject of great interest. The phenomenon appears to result from complex mechanisms, which involves microturbulence suppression by macroscopic sheared flows and/or magnetic chaos healing with formation of coherent magnetic structures. A satisfactory understanding of conditions in which transport barriers occur in such different toroidal magnetic configurations as the tokamak, the stellarator and the reversed-field pinch (RFP) is still lacking.

We describe here a first step in the application to magnetically confined plasmas of a technique developed for transport barrier diagnosis in ordinary incompressible fluids, where a divergence-free condition holds for the velocity field. The divergence free property of the magnetic fields provides the basis for the application of a similar technique in magnetically confined plasmas. The RFP, in particular, provides an optimal test bed for the application of this diagnostic tool since electron internal transport barriers (ITB) are presently believed to be governed by the magnetic field dynamics. In fact, ITBs form in experiments due to a global helical magnetic self-organization process which brings magnetic chaos healing in a relevant portion of the plasma volume [7, 8]. This self-organization process, which amounts to a global helical kinking of the toroidal plasma current and the ensuing process, consisting on the disappearence of the magnetic island X point and thus of a preferred region for magnetic chaos development, can be described in its basic features within 3D nonlinear magneto hydrodynamic modeling [9–11]. Numerical simulations will indeed provide the reference case for the work presented here.

Theoretical and numerical studies carried out up to now on the RFP magnetic topology rely heavily on the Poincaré plots. A Poincaré plot gives a detailed picture of the regular and chaotic domains of the magnetic field, provided one integrates the magnetic field equations starting from a sufficiently large number of initial conditions and for sufficiently large values of the parameter (position) along the field lines, that plays the role of an effective time. In this paper we will call this effective time the field-line-time or just time. When we refer to real or dynamic time, we will explicitly say so. However, Poincaré maps do not provide

information on the "transport" of the magnetic field lines, *i.e.* how the magnetic field lines migrate in field-line-time. In particular they do not allow to investigate on the possible presence inside the chaotic domains of surfaces that may act as barriers to the magnetic field line penetration on a given field-line-time scale. These structures are usually referred to as Lagrangian Coherent Structures (LCSs), especially in the hydrodynamic systems literature; in plasma literature, where Hamiltonian nonlinear dynamics has been perhaps more popular, similar bounds on transport have been identified as so-called cantori, i.e. the remnants (forming a Cantor set) of conserved structures (KAM tori) under perturbation [12].

The investigation of LCS has been recently addressed by analyzing magnetic configurations produced by numerical experiments of magnetic reconnection in collisionless plasmas within a generic 3D geometry [13–15]. In particular in Refs. [14, 15] a technique derived from fluid dynamics, based on the geometrical properties of the Finite Time Lyapunov Exponents (FTLE) of the magnetic field lines, has been used. Compared to the standard Lyapunov exponent that is defined for the time that goes to infinity, the FTLE measures the exponential separation between two neighboring field lines after a given amount of time. Within the context of FTLE theory, approximate Lagrangian Coherent Structures may be defined as second-derivative ridges of the scalar FTLE field [2]. Following [2] we define a ridge as a curve in the plane perpendicular to the field-line time direction where the gradient in the FTLE-field is parallel to the curve and the second derivative of the FTLE-field in the direction perpendicular to the curve is negative. As suggested in [2] this is in analogy with hiking: while hiking along a "ridge" one would expect to be *locally* at the highest point of the FTLE field transverse to the ridge and the curvature would be steepest downward transverse to the curve. The analysis carried out in [14, 15] addressed a partially chaotic magnetic configuration, where stochastic and regular domains coexist. In those cases the ridges of the FTLEs showed the presence in the chaotic regions of well-defined magnetic structures that act as temporary obstacles to the field line motion. A spectroscopic approach to the motion of magnetic field line allowed to evaluate the effectiveness of these barriers and to show that in the partly stochastic case a field line moves radially in steps. In each of these steps the magnetic field line lays in structures which are in relation with rational values of the winding number. This result, seemingly counterintuitive, seems strongly intertwined with the ITBs' characterization in magnetically confined fusion plasmas. Many authors analyzed the nature of these transport barriers in the framework of Hamiltonian dynamics study. In

[16, 17] the occurrence of strong transport barriers has been discussed in relation to the presence of magnetic resonances and magnetic shear. In the Tokamap mapping framework Misguich [18] has shown that the ITBs can be more precisely located on Cantori (irrational surfaces) with *noble* q values embedded between two rational surfaces, which are expected to correspond to less robust surfaces. Later Hudson [19, 20] has proposed a way to identify these Cantori through *ghost surfaces*, showing in the first work that the steepest temperature gradients coincide with these irrational surfaces.

In this paper we intend to adopt the same approach of refs. [14, 15] for analyzing a weakly stochastic magnetic field by simulating numerically a RFP state close to the quasi-single helicity (QSH) state, with the aim of identifying LCSs. In Section II we introduce the adopted numerical technique, performing a validation test, whose results highlight the reliability of the FTLE computation. A key feature of the considered scheme is the possibility to investigate realistic situations, where a numerical description of the magnetic field is generally available, conversely to previous work where analytical functions were needed. In Section III we describe the MHD equations model and the reference numerical case. Starting from an axis-symmetric equilibrium, the magnetic configuration evolves towards a QSH state. The results of the analysis, discussed in Section IV, show the presence of magnetic barriers recognized as the LCSs related to the magnetic field configuration: the LCSs are aligned along finite lengths manifolds, where the magnetic field lines show values in close relation with rational values of the winding number.

II. NUMERICAL METHODS

A. FTLE computation

As already stated, in this work the FTLE method has been applied to reveal the coherent structures in a magnetic configuration obtained from a numerical experiment simulating the characteristic behavior of the RFP confinement scheme. In the RFP the MHD dynamo activity provided by the resistive kink - tearing modes plays a major role in determining the magnetic topology variations. The analysis of magnetic field topology is tackled solving the magnetic field line equations. In cylindrical geometry the trajectory $(r(z; z_0, \mathbf{x_0}), \theta(z; z_0, \mathbf{x_0}))$ of the magnetic field line that passes through $r(z_0) = r_0, \theta(z_0) = \theta_0$, at each dynamical time

t, obeys the equation system:

$$\frac{dr}{dz} = \frac{B_r(r,\theta,z,t)}{B_z(r,\theta,z,t)} \tag{1}$$

$$\frac{d\theta}{dz} = \frac{1}{r}\frac{B_\theta(r,\theta,z,t)}{B_z(r,\theta,z,t)} \tag{2}$$

where B_r, B_θ, B_z are the magnetic field components along the radial r, the poloidal θ and the toroidal z directions, respectively. The above system describes in field-line time z what has been coined in fluid dynamics as chaotic advection, the magnetic field playing the role of the advecting velocity field.

The FTLE σ is defined by

$$\sigma(z, z_0, \mathbf{x}_0) = \frac{1}{|z - z_0|} \ln \sqrt{\lambda(z, z_0, \mathbf{x}_0)}, \tag{3}$$

$|z - z_0|$ being the length of the time the FTLE is computed and $\mathbf{x} \equiv (r, \theta)$. The quantity λ represents the maximum eigenvalue of the matrix

$$\Delta = \frac{d\phi^z_{z_0}(\mathbf{x})^*}{d\mathbf{x}} \frac{d\phi^z_{z_0}(\mathbf{x})}{d\mathbf{x}}, \tag{4}$$

where $\phi^z_{z_0}$ is the flow map that associates the initial position $\mathbf{x}_0$ at time z_0 to the final position $\mathbf{x}$ at time z according to the magnetic field line equations,

$$\phi^z_{z_0} : \mathbf{x}_0 \mapsto \phi^z_{z_0}(\mathbf{x}_0) = \mathbf{x}(z; z_0, \mathbf{x}_0). \tag{5}$$

The matrix $\frac{d\phi^z_{z_0}(\mathbf{x})}{d\mathbf{x}}$ denotes the Jacobian matrix of $\phi^z_{z_0}$ and $\frac{d\phi^z_{z_0}(\mathbf{x})^*}{d\mathbf{x}}$ its transpose. In the limit $|z - z_0| \to \infty$ the standard Lyapunov coefficient is obtained [21].

In Ref. [14] the FTLEs have been computed by numerically implementing the method derived in Ref. [22]. The key feature of this approach is an efficient decomposition of the tangent map, corresponding to the linear representation of $\phi^z_{z_0}$, through orthogonal matrices. This results in a set of coupled ordinary differential equations for the Lyapunov exponents along with the various angles parameterizing the orthogonal matrices. The system of differential equations is treated as an initial value problem and solved numerically to obtain the Lyapunov exponents. Despite the high precision level, a rather stringent constraint of this method is represented by the requirement of an analytical description of the magnetic field. In [14] it was possible to satisfy this requirement studying an academic case of 3D magnetic reconnection in a periodic configuration. This allowed to apply Fourier decomposition to

the magnetic field components and to consider just the higher amplitude modes for approximating the original data [13].

On the contrary, in the present work a global MHD numerical simulation is considered and the method of Ref. [22] cannot be used. For this reason the FTLE are now computed directly from the definition (3), which requires the knowledge of the flow map. To perform the analysis, the trajectories of magnetic field lines starting from a set of points regularly distributed on a grid is computed during the time interval $[z_0, z]$. Once the final positions of each field line is found, the spatial gradient of the flow map can be evaluated at each point in the initial grid by finite differencing with values at the neighboring grid points. In the case of a central difference method, adopted in this work, the formula for the gradient of the flow map at an arbitrary point (i, j) in the grid reads as

$$\left.\frac{d\phi^z_{z_0}(\mathbf{x})}{d\mathbf{x}}\right|_{\mathbf{x}_{i,j}} = \begin{pmatrix} \frac{r_{i+1,j}(z)-r_{i-1,j}(z)}{r_{i+1,j}(z_0)-r_{i-1,j}(z_0)} & \frac{r_{i,j+1}(z)-r_{i,j-1}(z)}{\theta_{i,j+1}(z_0)-\theta_{i,j-1}(z_0)} \\ \frac{\theta_{i+1,j}(z)-\theta_{i-1,j}(z)}{r_{i+1,j}(z_0)-r_{i-1,j}(z_0)} & \frac{\theta_{i,j+1}(z)-\theta_{i,j-1}(z)}{\theta_{i,j+1}(z_0)-\theta_{i,j-1}(z_0)} \end{pmatrix} \tag{6}$$

where $\mathbf{x}_{i,j}(z) = (r_{i,j}(z), \theta_{i,j}(z))$ are the coordinates of point (i, j) at time z. Once the quantity in eq.(6) is computed for each point of the grid, the matrix Δ is obtained by multiplying $\frac{d\phi^z_{z_0}(\mathbf{x})}{d\mathbf{x}}$ by its transpose. The computation of the largest eigenvalue of the 2x2 matrix Δ finally gives the FTLE at the point (i, j) through the formula (3).

In order to verify its reliability, we adopted this new approach for computing the FTLEs of the earlier magnetic configuration reported in Ref. [14], at the so-called "transition to the global stochasticity" phase. Fig. 1 shows the comparison between the result we obtained (red lines) and the FTLE field computed with the method described in Ref. [22]. We focused on a small subdomain, compared to the original box showed in Ref. [14], where chaotic and regular regions coexist. The finite time over which the Lyapunov exponents have been calculated is the same in both cases and equal to $z = 12L_z$, where L_z is the periodicity length along the toroidal direction. Moreover, two different initial condition distributions have been used in order to check the convergence of the FTLE calculation, based on the study of the flow map, to the one obtained in Ref. [14]. In particular, the two distributions are generated by sampling uniformly on 300×200 (fig. 1a) and 600×300 (fig. 1b) points. Figure 1, which show the linear plot of the FTLE field along the radial position x for $y = 0$, highlight the quite similar behavior of the two approaches. In both graphs, red and black curves show the presence of highly spiky regions ($0.4 < x < 0.42$ and $0.44 < x < 0.48$), that correspond to the areas where the magnetic field is most stochastic. In the remaining part

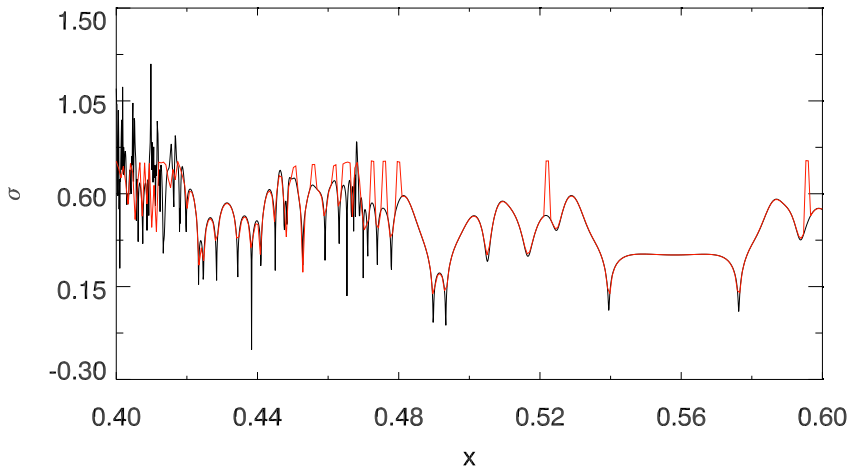

(a)

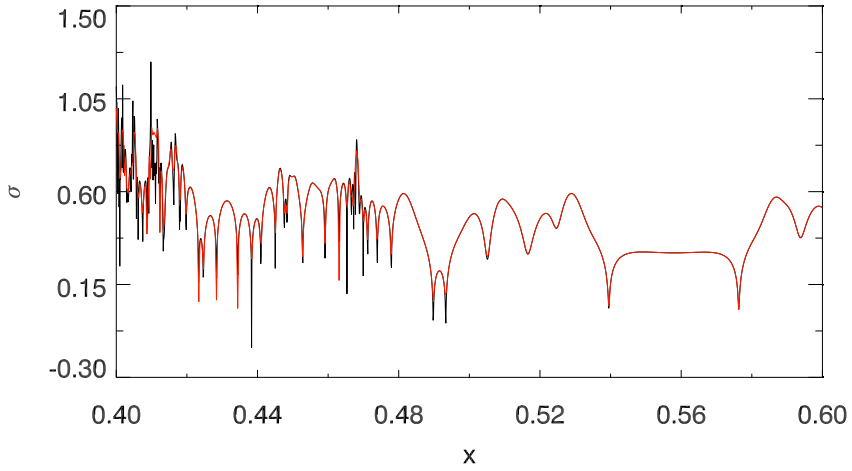

(b)

FIG. 1: Profiles of the FTLE field σ along x, for $y = 0$. Red curves have been computed using the formula 3 at $z = 12L_z$ with two different uniform distributions of the initial conditions in the domain $0.4 < x < 0.6$ and $-0.25 < y < 0.25$: (a) 300 $\times$ 200 and (b) 600 $\times$ 300. Black curves have been obtained using the method described in [14].

of the considered domain, however, the FTLE profiles are rather regular, with extremely sharp gradients. Here the FTLE distribution is characterized by the presence of ridges, which identify the LCS confining the magnetic field lines. Comparing the figures 1a and 1b, the role of the mesh resolution is clearly visible. In fact, increasing by a factor of three the number of initial conditions, more accurate results have been obtained, and the FTLE

fields practically coincide with the one computed with the analytical approach, especially in regions characterized by a quite smooth behavior.

B. LCS extraction

A definition of a LCS of the magnetic field configuration can be based upon the FTLE. As in Ref. [14], our analysis follows the method discussed in Ref. [2, 3], where the Lagrangian coherent structures of a velocity field are defined as ridges of FTLE field of the corresponding particle trajectories. In particular the "second derivative ridge" definition is assumed, which relies on the Hessian of the FTLE field. In the case of magnetic fields, we define a LCS as a ridge in the FTLE-field of the field line trajectories.

A ridge is a curve $\mathbf{c}(s)$ (s being the parameter along the curve) that satisfies two requirements:

1. The gradient in the FTLE-field is along the curve. This means that the tangent vector $\mathbf{c}'(s)$ and $\nabla\sigma(\mathbf{c}(s))$ have to be parallel.

2. $\Sigma(\mathbf{n},\mathbf{n}) < 0$ is minimal, where $\mathbf{n}$ is the unit normal vector to the curve $\mathbf{c}(s)$ and Σ is the Hessian, evaluated at the point $\mathbf{c}(s)$.

To extract the LCS from the FTLE field, both the Hessian of the FTLE, $\Sigma = \frac{d^2\sigma(\mathbf{x})}{d\mathbf{x}^2}$, and the gradient lines $\nabla\sigma$ are determined. In the case of the Cartesian grid we adopted, both have been easily computed from finite-differencing. Once the eigenvectors corresponding to the minimum eigenvalue direction of the Hessian are computed, a scalar field can be formed by taking the inner product of these eigenvectors with the gradient field. Then ridges are extracted by looking at the zero-valued level sets. When chaotic "flows" are taken into account, as in the case of the magnetic fields we consider here, the influence of the numerical noise on the computation of the ridges can become an issue. In order to remove these spurious effects, we have chosen a natural, easy to implement, criterion which prescribes a minimum height of the ridge and of the FTLE gradient field.

Fig.2 shows the FTLE ridges of the partially chaotic magnetic configuration described in Ref. [14] we discussed above. Green lines correspond to the ridges extracted from the FTLE distributions computed with the method based on the direct evaluation of the flow map for both the considered meshes. Red curves refers to the FTLE field obtained with the technique adopted in Ref. [14]. The two sets of curves are in quite good agreement,

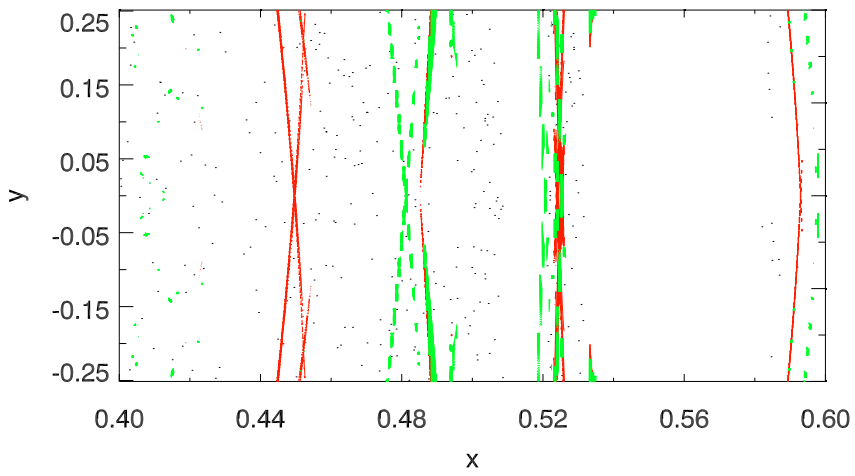

(a)

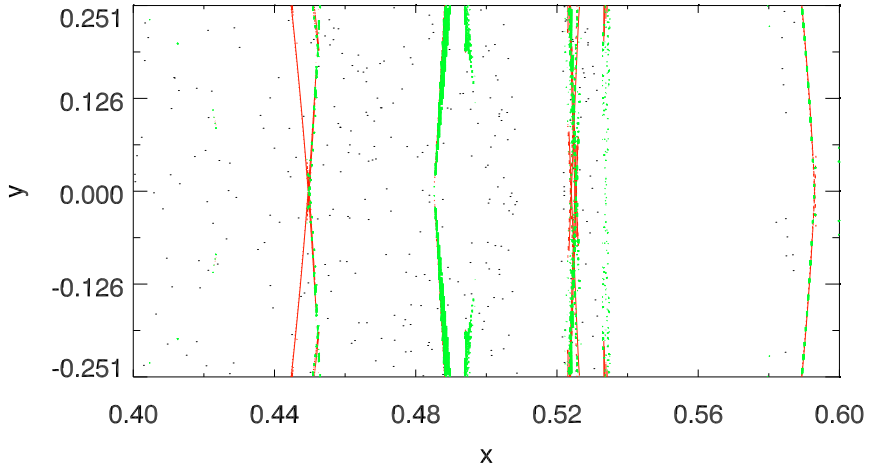

(b)

FIG. 2: Ridges extracted from the FTLE field computed with the method based on the study of the flow map on the $x - y$ subdomain $[0.4, 0.6] \times [-0.25, 0.25]$ (green lines) with two different samplings: (a) 300×200 and (b) 600×300 points. The ridges extracted from the FTLE field obtained with the method adopted in [14] are also shown (red lines).

particularly in fig. 2b. Observing fig. 2a, on one hand small misalignments emerge, and on the other hand the detection of the LCSs is incomplete, since the ridge on the left ($x < 0.46$) is not identified. This behavior is due to the different spatial resolution adopted in the two FTLE computations, as can be seen by comparing the two figures. All the tests discussed

above prove the FTLE computation adopted in this work is reliable and suitable for treating general magnetic configuration, provided a large enough number of initial conditions is used.

III. MAGNETIC FIELD DESCRIPTION OF THE RFP REFERENCE CASE

In the following the study of the coherent magnetic structures that emerge during the nonlinear stages of a reconnection process in a RFP confinement scheme is presented. The dynamics of this process is provided by a numerical simulation [23] carried out with the code SpeCyl [24], which proved to catch several aspects of the experimental phenomenology (see for example the recent letter [25] and therein references). SpeCyl solves the 3D nonlinear visco-resistive MHD equations in a periodic cylinder (rectified torus) with radial coordinate r, azimuthal (poloidal) coordinate θ and axial (toroidal) coordinate z with a period of $2\pi R_0$. The aspect ratio of the rectified torus is set to $R_0 = 4$. The model's equations, in dimensionless form, are given by:

$$\frac{\partial \mathbf{v}}{\partial t} + \mathbf{v} \cdot \nabla \mathbf{v} = \mathbf{J} \times \mathbf{B} + \nu \nabla^2 \mathbf{v} \tag{7}$$

$$\frac{\partial \mathbf{B}}{\partial t} = \nabla \times (\mathbf{v} \times \mathbf{B} - \eta \mathbf{J}) \tag{8}$$

$$\nabla \times \mathbf{B} = \mathbf{J} \tag{9}$$

$$\nabla \cdot \mathbf{B} = 0 \tag{10}$$

where $\mathbf{B}$ is the magnetic field, $\mathbf{J}$ the current density, and $\mathbf{v}$ the plasma velocity field. The adimensional parameters $\eta = S^{-1}$, where S is the Lundquist number, and $\nu = M^{-1}$, where M is the viscous Lundquist number, represent the plasma resistivity and viscosity, respectively. The initial condition of the dynamical simulation is the so-called "1D ohmic equilibrium", obtained from eq. 7 by imposing $\frac{\partial}{\partial t} = 0$ and $\mathbf{v} = 0$, adding Ohm's law [26]. Fig. 3 shows the radial profiles of some relevant quantities at the initial equilibrium.

In order to induce the magnetic relaxation to mean reversed field typical of the RFP two linearly unstable helical perturbations are imposed on the initial axis-symmetric equilibrium. The Fourier transforms of the perturbed fields along the poloidal and toroidal direction are characterized by the mode number $m_1 = 1, n_1 = -9$ and $m_2 = 1, n_2 = -10$. They produce two magnetic island chains resonating at different spatial position $\chi = const$, where χ is the helical flux function defined as $\mathbf{B} \cdot \nabla \chi = 0$. The Lundquist number is $S = 3 \times 10^4$ while the

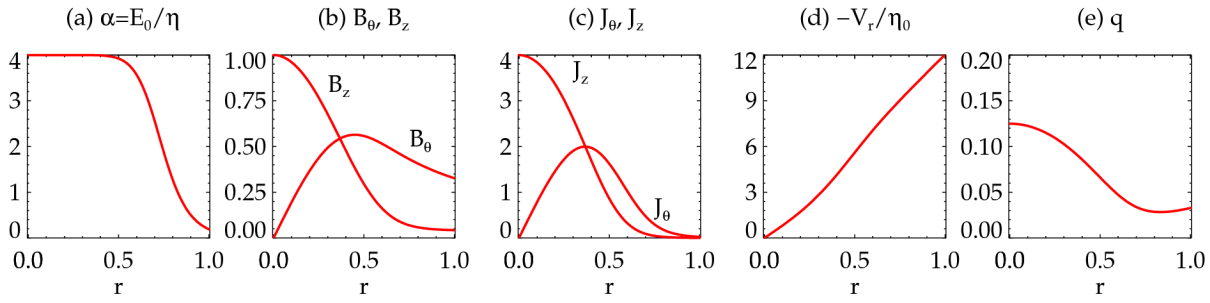

FIG. 3: Initial equilibrium radial profiles for some significant quantities.

magnetic Prandtl number $P = \frac{\nu}{\eta}$ is set to $P = 10^3$. The dynamics of the process is shown in fig. 4 where the temporal evolution of the magnetic energy of the main $m = 1$ modes is reported. The $n = -9$ mode, the most unstable between the two perturbed modes, is the dominant mode in the second part of the linear growth phase and at the beginning of the nonlinear saturation phase, when the other $m = 1$ modes arise. The nonlinear dynamics makes the $n = -10$ mode to become the dominant one after $t = 2000\tau_A$. The exponential decay of the secondary modes brings the system to the final $n = -10$ single helicity (SH) equilibrium configuration.

The specific SpeCyl simulation we consider for this first application is a schematic yet paradigmatic case of magnetic chaos healing in RFP [11], which has been discussed in its general features in [23]. The highlights are as follows. In a first stage, starting around $t = 600\tau_A$, a macroscopic chaotic region appears between the two magnetic islands induced by the initial perturbations and, in particular, inside the separatrix of the $n = -9$ mode. As time increases, the chaotic volume increases together with the island widths, according to the Chirikov criterion [27]. Later on, at $t = 750\tau_A$, the amplitude of the $n = -9$ is so large that the separatrix expulsion occurs, which is seen by disappearance of the helical axis. Then, at $t = 790\tau_A$, chaos is strongly reduced in the whole domain. It only survives at the separatrix of the outer $n = -10$ island, which reappears with a rather elongated shape at this time. The chaos healing effect is robust and lasts for a long time, even if the amplitude of secondary modes is increasing. At $t = 1800\tau_A$, for instance, well defined magnetic surfaces are still observed in the whole domain, either closed around the helical axis or in the form of secondary islands.

The analysis of the magnetic field topology during the evolution of the reconnection process has been carried out by the field line tracing code NEMATO [28, 29]. Once the magnetic

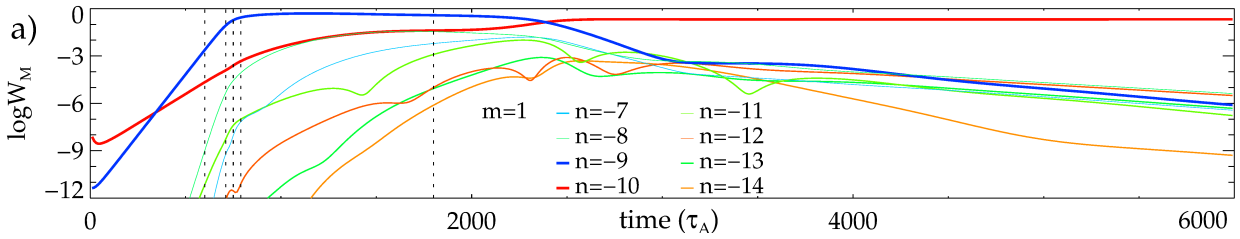

FIG. 4: The temporal evolution of the magnetic energy of the main m = 1 modes. The time t is expressed in terms of the Alfvè time τ_A. Vertical bars mark the times $t = 600, 750, 790, 1800$.

field at a fixed dynamic time t is provided, NEMATO solves the magnetic field line equations in the parametric form, $\frac{d\mathbf{x}}{d\tau} = \mathbf{B}(\mathbf{x}, t)$, on the 3D grid $\mathbf{x}$, where τ is a parameter along the field lines. It has been verified that this code is particularly suitable to study weakly chaotic magnetic fields typical of the quasi-single helicity state in RFP. This is due to two main features: the interpolation scheme, which ensures the solenoidal nature of the field everywhere in the domain, and the volume-preserving integration scheme. Together, they exactly preserve $\nabla \cdot \mathbf{B} = 0$ to numerical round-off along each magnetic field line.
The magnetic field line trajectories computed by NEMATO can be visualized through Poincaré maps on the poloidal sections $\theta = const$ or on the toroidal planes $z = const$. This provides a glimpse of the magnetic field topology at a desired dynamical time t during the numerical simulation performed by SpeCyl.

IV. MAGNETIC TRANSPORT BARRIERS IN A QUASI-HELICAL (QSH) CONFIGURATION

In this work we apply the FTLE analysis for the detection of transport barriers on a magnetic configuration in the QSH state. In particular, we focused on the time $t = 600\tau_A$ of the MHD simulation reported in fig. 4. It is worth noting, in fact, that at this dynamical time the magnetic configuration is strongly dominated by a single helicity, the $(1, -9)$ mode, whose amplitude is two order of magnitude larger than the amplitude of the $(1, -10)$ mode. The Poincaré map in fig. 5 shows the topology of the corresponding magnetic field on the poloidal section $z = 0$. It has been obtained by integrating a set of 256 magnetic field lines up to the field-line time $z = 1000L_z$ by the NEMATO code. The magnetic field

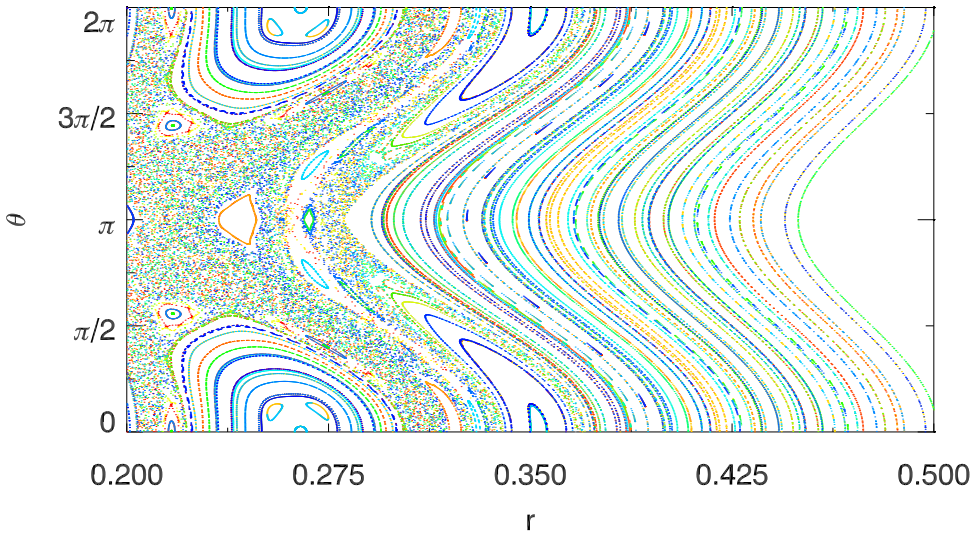

FIG. 5: Poincaré map on the $z = 0$ section of the magnetic field at $t = 600\tau_A$. The field lines trajectories have been obtained by the NEMATO code starting from a set of 256 initial conditions uniformly distributed on a 16×16 mesh, where $0 \leq \theta \leq 2\pi$ and $0.2 \leq r \leq 0.45$. The integration has been carried out up to $z = 1000L_z$.

lines are initially distributed over a uniform 16×16 mesh on the domain $0.2 \leq r \leq 0.45$, $0 \leq \theta \leq 2\pi$. Two rather large regions with regular KAM surfaces, floating in the stochastic sea, are visible. They represents the remnants of the magnetic islands induced by the initial perturbations $(1, -9)$ and $(1, -10)$, whose O-points are centered around $(0.25, 0)$ and $(0.35, 0)$ respectively. Smaller magnetic islands are also present, caused by the beating of the two main perturbations.

The FTLE field for this system has been calculated for a set of 3.44×10^7 magnetic field lines initially distributed at $z = 0$ over a uniform 4096×8400 mesh on the domain $0.2 < r < 0.45$, $0 < \theta < 2\pi$. Fig. 6 shows the results after 10 iterations along the toroidal direction, which corresponds to $|z - z_0| = 10L_z = 80\pi$. It is important to point out that the determination of a suitable integration time in the FTLE definition is a critical issue, as it naturally depends on the specific case. As shown in Ref. [2] one must carefully choose an integration time large enough to allow a sufficient separation of the field lines. On the other hand, we have assumed that the field lines stretching is described by the derivative of the flow map: this assumption is valid for an infinitesimal initial separation and, if z is large and the grid spac-

ing is not sufficiently small, it could break down. A comparison of different results obtained with different integration times has been carried out. The choice $|z - z_0| = 10L_z$ has been considered as a suitable value since the corresponding structures well matches the essential features of the topology of the considered magnetic configuration.

The FTLE distribution clearly exhibits extremely sharp gradients, corresponding to ridges, inside the chaotic area. On the contrary, in the regular regions, both inside and outside the stochastic domain, the FTLEs have a quite smooth behavior and small values. Finally, thin layers, where the FTLE field is rather spiky, can be observed around the island patterns related with the modes $(1, -9)$ and $(1, -10)$.

Second derivative ridges in this FTLE field are extracted according to the algorithm described in sec.2 and are shown in fig. 7 (black curves) together with the Poincaré map. Well defined ridges are distributed along the external borders that enclose the chaotic region. This is not surprising because these borders are regular magnetic surfaces that correspond, by definition, to LCSs and as a consequence to the ridges of the FTLE, according to Ref. [2]. More interestingly, fig .7 shows that ridges do exist also in the middle of the stochastic domain.

As in Ref. [14] we can prove these structures correspond to the invariant manifolds that emanate from special hyperbolic points. These points are the intersections of the so-called "distinguished" hyperbolic lines (the generalized X-lines) [13] with the $z = 0$ plane. Fig.8 shows the LCSs (black lines) with superimposed the manifolds rising at $(0.256, \pi)$ (red line), $(0.2635, \pi)$ (light blue line) and $(0.277, \pi)$ (green line). The manifolds are computed by plotting the Poincaré maps of a set of magnetic field lines initially distributed on a close curve centered around the corresponding hyperbolic points. This method is a simplified version of the rigorous contour-dynamic technique [30], which can become not convenient when chaotic fields are considered due to the high computational costs. In order to map both the unstable, or repelling, manifold and the stable, or attracting, manifold magnetic field line equations have been integrated forward and backward in time z, respectively. For each hyperbolic point, we considered a set of 1024 initial conditions uniformly distributed along the sides of a square whose width is $L = 2 \times 10^{-4}$. The manifolds rising at $(0.256, \pi)$ have been traced up to $|z| = 20L_z$, while for the other two hyperbolic points the magnetic field line integration has been carried out up to $|z| = 25L_z$. The figure shows that the ridges tend to be aligned with and practically coincide with the branches of the corresponding

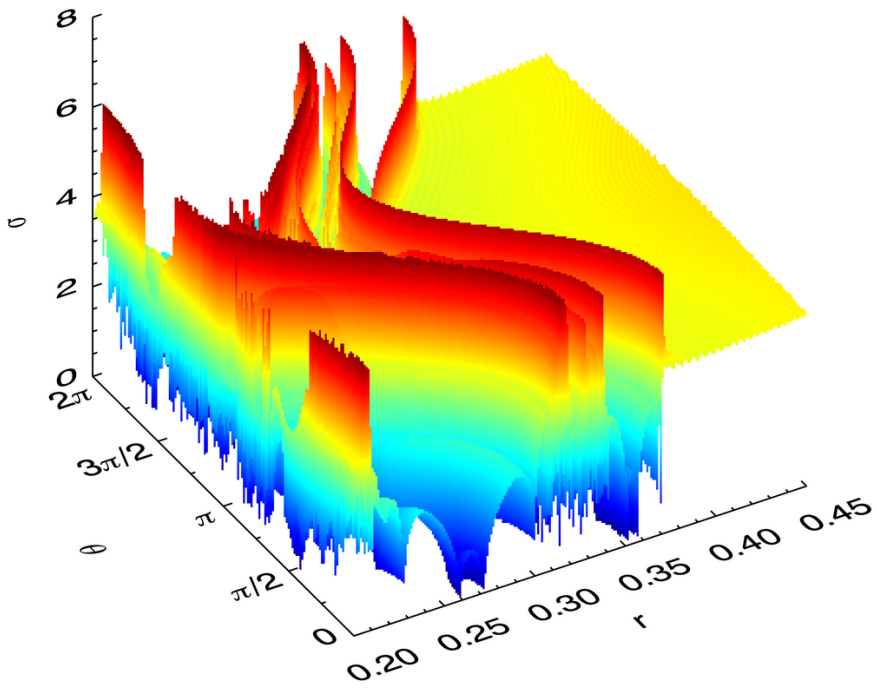

FIG. 6: FTLE field obtained with a set of 4096×8400 initial conditions uniformly distributed on the domain $[0.2, 0.45] \times [0, 2\pi]$. The integration time has been set to $z = 10L_z$.

stable and unstable manifolds, which are computed for a few L_z periods. It is seen that magnetic field lines hardly cross these manifolds, thus FTLE ridges form an actual barrier with respect to magnetic field line transport.

In fig. 9 we have overplotted the FTLE ridges on the Poincaré map on the $z = 0$ plane produced, after 1000 toroidal iterations, by two set of magnetic field lines whose initial conditions are randomly distributed on the left (red area) and on the rigth (green area) of the red manifold of fig. 8. It is clearly visible that the ridges associated to this manifold prevent for a quite long time interval the transport of field lines from the stochastic area in red into the green stochastic region, and vice versa. These ridges act therefore as effective transport

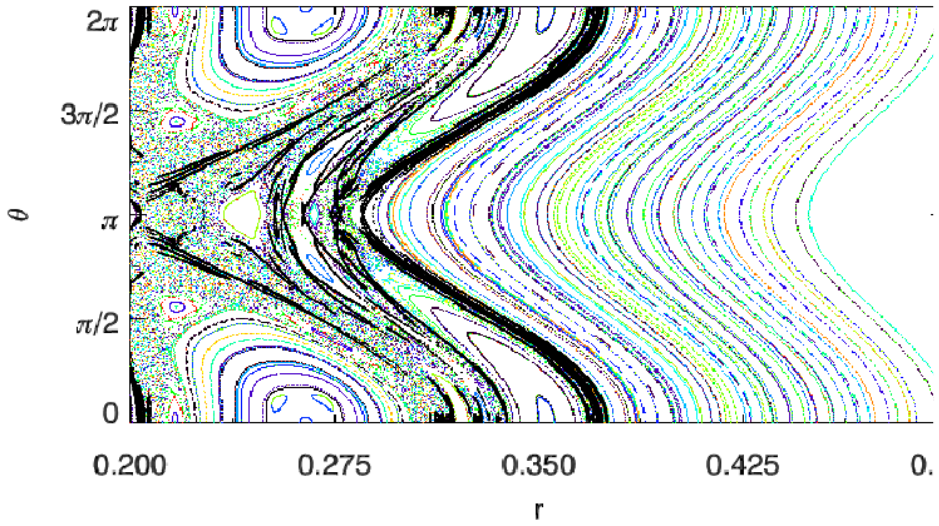

FIG. 7: Ridges (black curves) extracted from the FTLE field shown in fig. 6.

barriers against the magnetic field line penetration.

As shown in Ref. [15], each LCS is characterized by a specific rational number of the parameter ι, the so-called *rotational transform*. It represents the frequency oscillation of the hyperbolic line from which the LCS arises. It is well known that in the case of an axisym-

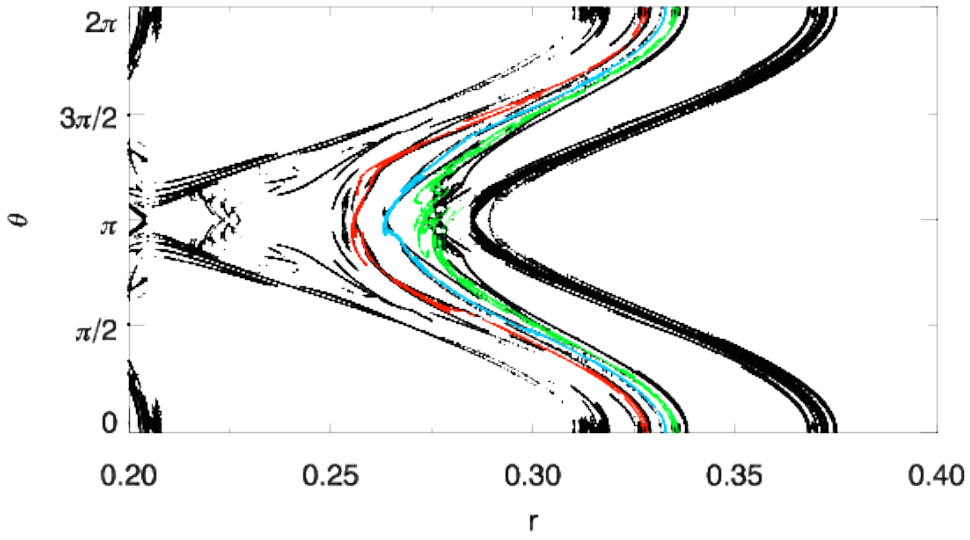

FIG. 8: Ridges extracted from the FTLE field (black lines) with superimposed the manifolds rising at $(0.256, \pi)$ (red line), $(0.2635, \pi)$ (light blue line) and $(0.277, \pi)$ (green line). Red manifold is traced up to $z = 20L_z$, while both the light blue and green manifolds are traced up to $z = 25L_z$. The three manifolds have been obtained with a set of 1024 initial conditions, centred on the corresponding hyperbolic points, uniformly distributed on a square in the (r, θ) plane of side $L = 2 \times 10^{-4}$.

metric system ι corresponds to the inverse of the safety factor, $1/q = RB_\theta/rB_z$. According to eq.2 q can be written as

$$q = \frac{d\phi}{d\theta} \tag{11}$$

where $\phi = dz/R$.

To compute the characteristic frequency of the magnetic barrier highlighted in fig. 9 we followed the trajectory of a magnetic field line starting around the hyperbolic point $(0.256, \pi)$ for a time interval during which the field line remains trapped on the corresponding coherent structure. An example of the characteristic behavior is shown in fig. 10, where the θ coordinate is plotted versus the ϕ coordinate. The result is a set of straight lines whose slope is constant and equal to 0.10512, close to the rational number 2/19. This means that the considered magnetic field line describes a trajectory that travels $m = 2$ poloidal laps each $n = 19$ toroidal laps. It is worth to note that this result agrees with the radial profile of the safety factor, numerically measured in Ref. [23]. The oscillation frequency is

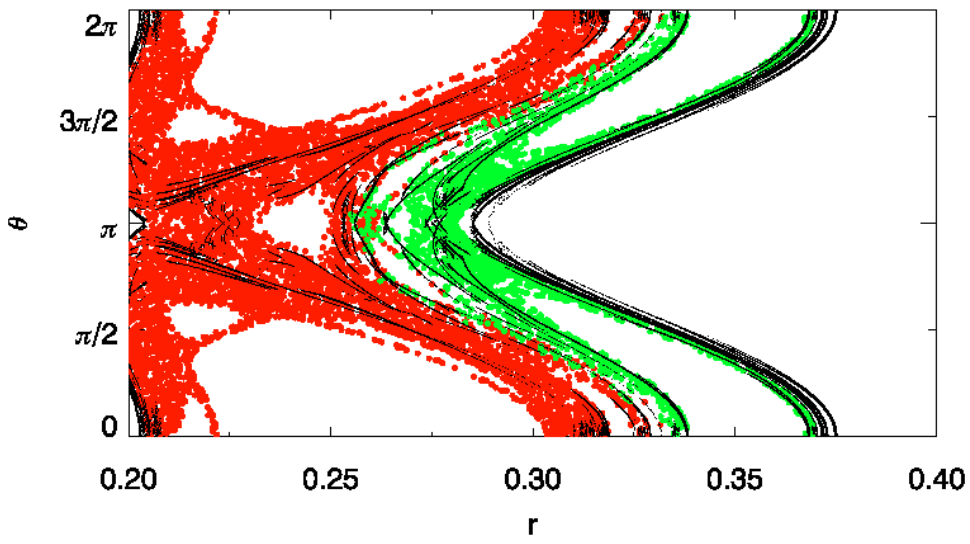

FIG. 9: Poincaré map of two sets of initial conditions randomly distributed on the left (red area) and on the right (green area) of the red manifold in fig. 8. This map has been obtained with a set of 20 initial conditions in the red area and 12 initial conditions in the green area. The black curves represent the ridges extracted from the FTLE field. The field-line time integration for the Poincaré map is $z = 1000L_z$.

also consistent with the spatial position where the detected magnetic structure is centered. Since it is located between the rational surfaces of the primary modes $m_1 = 1, n_1 = -9$ and $m_2 = 1, n_2 = -10$, the corresponding wave numbers satisfy the condition:

$$|mn_i - m_i n| = 1. \tag{12}$$

A more precise identification of such structures in terms of winding number and noble cantori (following [18, 19]) is out of the scope of this paper and is left for future work.

V. CONCLUSIONS

In this paper we report the first application of the Finite Time Lyapunov Exponent method for analyzing the topology of a magnetic field resulting from 3D nonlinear MHD simulations of the RFP. We focused on the magnetic field at a fixed dynamical time, corresponding to a state when a quasi-single helicity state arises. This is a partially chaotic configuration, characterized by the presence of a dominant MHD mode that starts to impress

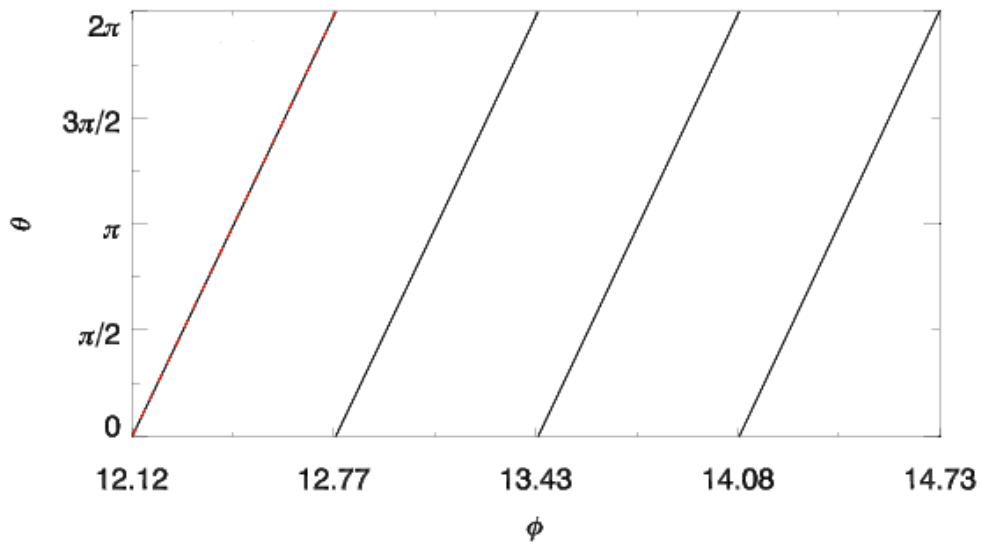

FIG. 10: Evolution of the poloidal coordinate θ as a function of the toroidal coordinate ϕ for a field line initially located at the hyperbolic point $(0.256, \pi)$.

a 2D helical symmetry to the plasma column. The intrinsically 3D nature of the field results in the presence of a domain characterized by the presence of stochastic magnetic field lines. The aim of this analysis is to evaluate the possible presence in the chaotic domain of Lagrangian Coherent Structures, defined as ridges of the FTLE distribution, which can act as barrier for the magnetic field line transport. Such barriers could influence the self-organization process and play a fundamental role on the appearance of the QSH state observed in RFP experiments.

Compared to previous analysis, where just an analytical description was available for the magnetic field distribution, a new approach for the computation of the FTLE has been reported that is suitable to be applied to configurations from numerical modeling and experimental cases.

As a first step the reliability of the new approach was verified: the new results showed an excellent degree of agreement with the ones coming from the previous analytical description of the magnetic field.

As a second step we analyzed the magnetic field coming from the 3D nonlinear MHD code SpeCyl and analyzed by the NEMATO field line tracing code. Well defined chains of FTLE ridges have been identified. Some of the ridges lie inside the chaotic regions of the Poincaré

plots and we have verified through the analysis of the behavior of a sample of magnetic field lines that these structures act as effective magnetic barriers preventing magnetic field line transport across them. When a magnetic field line is trapped by such a structure it exhibits an oscillation frequency close to the one of the corresponding hyperbolic trajectory. The authors speculate that these structures can be associated with noble cantori existing between two destroyed KAM tori, which are expected to provide important transport barriers for the magnetic field lines.

Despite the preliminary character of this work, the analysis we carried out can provide new insights into the dynamics of the magnetic field observed in RFP configurations. In particular the structures emerging from the ridges of the FTLE field can be identified as a precursor signal for the onset of magnetic configuration, as the SHAx state. A deeper analysis, based on the inspection of different magnetic configurations, is foreseen to verify this conjecture.

ACKNOWLEDGMENTS

One of the authors (S.C.) would like to acknowledge useful discussions with Dominique F. Escande.

[1] G. Haller, Annual Review of Fluid Mechanics **47**, 137 (2015).

[2] S. Shadden, F. Lekien, and J. Marsden, Phys. D **212**, 271 (2005).

[3] M. Mathur, G. Haller, T. Peacock, J. E. Ruppert-Felsot, and H. L. Swinney, Phys. Rev. Lett. **98**, 144502 (2007).

[4] T. Tala, X. Garbet, and contributors, C. R. Physique **7**, 622 (2006).

[5] J. Connor, T. Fukuda, X. Garbet, C. Gormezano, V. Mukhovatov, M. Wakatani, the ITB Database Group, the ITPA Topical Group on Transport, and Internal Barrier Physics, Nuclear Fusion **44**, R1 (2004).

[6] K. H. Burrell, Physics of Plasmas **4**, 1499 (1997).

[7] M. Gobbin, P. Franz, R. Lorenzini, I. Predebon, A. Ruzzon, A. Fassina, L. Marrelli, B. Momo, and D. Terranova, Plasma Physics and Controlled Fusion **55**, 105010 (2013).

[8] R. Lorenzini, E. Martines, P. Piovesan, D. Terranova, P. Zanca, M. Zuin, A. Alfier, D. Bonfiglio, F. Bonomo, A. Canton, S. Cappello, L. Carraro, R. Cavazzana, D. Escande, A. Fassina, P. Franz, M. Gobbin, P. Innocente, L. Marrelli, R. Pasqualotto, M. Puiatti, M. Spolaore, M. Valisa, N. Vianello, and P. Martin, Nature Physics **5**, 570 (2009).

[9] S. Cappello and R. Paccagnella, Physics of Fluids B **4**, 611 (1992).

[10] S. Cappello and D. F. Escande, Phys. Rev. Lett. **85**, 3838 (2000).

[11] D. F. Escande, R. Paccagnella, S. Cappello, C. Marchetto, and F. D'Angelo, Phys. Rev. Lett. **85**, 3169 (2000).

[12] R. MacKay, J. Meiss, and I. Percival, Physica D **13**, 55 (1984).

[13] D. Borgogno, D. Grasso, F. Pegoraro, and T. J. Schep, Physics of Plasmas **15**, 102308 (2008).

[14] D. Borgogno, D. Grasso, F. Pegoraro, and T. J. Schep, Physics of Plasmas **18**, 102307 (2011).

[15] D. Borgogno, D. Grasso, F. Pegoraro, and T. J. Schep, Physics of Plasmas **18**, 102308 (2011).

[16] M.-C. Firpo and D. Constantinescu, Physics of Plasmas **18**, 032506 (2011).

[17] L. Nasi and M.-C. Firpo, Plasma Physics and Controlled Fusion **51**, 045006 (2009).

[18] J. Misguich, J. Reuss, D. Constantinescu, G. Steinbrecher, M. Vlad, F. Spineanu, B. Weyssow, and R. Balescu, Plasma Phys. Control. Fusion **44**, L29 (2002).

[19] S. R. Hudson and J. Breslau, Phys. Rev. Lett. **100**, 095001 (2008).

[20] S. R. Hudson and Y. Suzuki, Physics of Plasmas **21**, 102505 (2014).

[21] J. P. Eckmann and D. Ruelle, Rev. Mod. Phys. **57**, 617 (1985).

[22] G. Rangarajan, S. Habib, and R. D. Ryne, Phys. Rev. Lett. **80**, 3747 (1998).

[23] D. Bonfiglio, M. Veranda, S. Cappello, L. Chacón, and G. Spizzo, Journal of Physics: Conference Series **260**, 012003 (2010).

[24] S. Cappello and D. Biskamp, Nuclear Fusion **36**, 571 (1996).

[25] D. Bonfiglio, M. Veranda, S. Cappello, D. F. Escande, and L. Chacón, Phys. Rev. Lett. **111**, 085002 (2013).

[26] D. Bonfiglio, L. Chacón, and S. Cappello, Physics of Plasmas **17**, 082501 (2010).

[27] B. Chirikov, J. Nucl. Energy Part C: Plasma Phys. **1**, 253 (1960).

[28] J. Finn and L. Chacón, Physics of Plasmas **12**, 054503 (2005).

[29] G. Ciaccio, M. Veranda, D. Bonfiglio, S. Cappello, G. Spizzo, L. Chacón, and R. B. White, Physics of Plasmas **20**, 062505 (2013).

[30] P. Vosbeek and R. Matthey, Journal of Computational Physics **133**, 222 (1997).